Fabrication of scalable and structured tissue engineering scaffolds using water dissolvable sacrificial 3D printed moulds

Mohanty, Soumyaranjan; Larsen, Layla Bashir; Trifol Guzman, Jon; Szabo, Peter; Burri, Harsha Vardhan Reddy; Canali, Chiara; Dufva, Martin; Emnéus, Jenny; Wolff, Anders

Published in:
Materials Science and Engineering C: Materials for Biological Applications

Link to article, DOI:
10.1016/j.msec.2015.06.002

Publication date:
2015

Document Version
Publisher's PDF, also known as Version of record

Materials Science and Engineering C 55 (2015) 569–578

Contents lists available at ScienceDirect

Materials Science and Engineering C

journal homepage: www.elsevier.com/locate/msec

Fabrication of scalable and structured tissue engineering scaffolds using water dissolvable sacrificial 3D printed moulds

Soumyaranjan Mohanty [a], Layla Bashir Larsen [a], Jon Trifol [b], Peter Szabo [b], Harsha Vardhan Reddy Burri [a], Chiara Canali [a], Marin Dufva [a], Jenny Emnéus [a], Anders Wolff [a,*]

[a] DTU Nanotech, Department of Micro- and Nanotechnology, Technical University of Denmark, Ørsteds Plads, DK-2800 Kgs. Lyngby, Denmark
[b] Danish Polymer Centre, Department of Chemical and Biochemical Engineering, Søltofts Plads, Building 229, DK-2800 Kgs. Lyngby, Denmark

ARTICLE INFO

Article history:
Received 23 February 2015
Received in revised form 7 May 2015
Accepted 4 June 2015
Available online 9 June 2015

Keywords:
Tissue engineering
3D printing
Scalable
PVA

ABSTRACT

One of the major challenges in producing large scale engineered tissue is the lack of ability to create large highly perfused scaffolds in which cells can grow at a high cell density and viability. Here, we explore 3D printed polyvinyl alcohol (PVA) as a sacrificial mould in a polymer casting process. The PVA mould network defines the channels and is dissolved after curing the polymer casted around it. The printing parameters determined the PVA filament density in the sacrificial structure and this density resulted in different stiffness of the corresponding elastomer replica. It was possible to achieve 80% porosity corresponding to about 150 cm^2/cm^3 surface to volume ratio. The process is easily scalable as demonstrated by fabricating a 75 cm^3 scaffold with about 16,000 interconnected channels (about 1 m^2 surface area) and with a channel to channel distance of only 78 μm. To our knowledge this is the largest scaffold ever to be produced with such small feature sizes and with so many structured channels. The fabricated scaffolds were applied for in-vitro culturing of hepatocytes over a 12-day culture period. Smaller scaffolds (6 × 4 mm) were tested for cell culturing and could support homogeneous cell growth throughout the scaffold. Presumably, the diffusion of oxygen and nutrient throughout the channel network is rapid enough to support cell growth. In conclusion, the described process is scalable, compatible with cell culture, rapid, and inexpensive.

1. Introduction

In recent years, there has been a great demand for the development of bioartificial organs/tissues in the field of organ transplantation and in vitro toxicological drug screening [1]. One of the primary challenges in translation of tissue engineering to clinical application is the difficulty in scaling up complex, biological effective tissues and organs to the size relevant for human [2]. Although small scale three-dimensional (3D) scaffold constructs have been achieved to mimic organs for e.g., in vitro drug testing [3], the applied fabrication approaches are not easily translated to constructs of human organ size. When engineering tissues in vitro, there is a requirement for structures or scaffolds that are able to support cell growth and at the same time mimicking the physiological environment including the geometrical, topographical and physical features of the targeted tissue. Specifically for the generation of thick 3D tissues, the development of highly dense vascular networks that can meet the nutrient and oxygen requirements of large masses of living cells remains a tissue engineering challenge. This often limits the size of engineered tissues to a few hundred micrometres [4]. The ideal tissue engineering scaffold supports the spatial distribution of cells in a three dimensional structure, provides mechanical stability to the cells and enables optimum nutrient transport and metabolic waste removal [5,6]. Numerous approaches exist to create 3D highly vascularized engineered tissue scaffolds to accommodate a high density of cells in high surface to volume ratio structures [6,7]. One strategy has been to use highly porous structures with interconnected pores/microchannels that provide space for penetration and growth of cells and enable favourable mass transport characteristics [8,9]. The structural, mechanical and mass transport properties of such scaffolds are determined by parameters such as pore size, pore shape, porosity, pore interconnectivity, permeability, scaffold surface area, scaffold effective stiffness and scaffold material [10].

Scaffolds consisting of stochastic, disordered or random micropores are one of the oldest and most widely used templates for tissue engineering [11,12]. Manufacturing techniques such as solvent casting-particulate leaching [13], phase separation [14], gas foaming [15], emulsion freeze drying [16] and fibre meshes [17] have been used to generate engineered scaffolds of foam-like internal structure with a random architecture and a limited control of scale [18]. Although such processing techniques are quick, scalable and economical, they do not enable accurate control of the microarchitectural details such as the

* Corresponding author.
E-mail address: anders.wolff@nanotech.dtu.dk (A. Wolff).

http://dx.doi.org/10.1016/j.msec.2015.06.002

pore size, geometry, their interconnections and distribution within the scaffold [19]. The possibility to control the inner architecture of scaffolds is desirable as it enables the control over its mechanical strength, the effective surface area for cell growth, and nutrient flow profiles within the scaffold [18]. To produce scaffolds with fine control over scaffold architecture in three dimensions, layer-by layer assembly techniques, where layers of polymers, patterned by moulding or embossing processes, are stacked, have been investigated by many researchers [20,21]. These techniques enable the formation of channels with precisely defined dimensions. However, the requirement for microfabricated master moulds and manual alignment of layers implies a slow and tedious process for achieving a multi-layered 3D construct [22].

Recently there has been a move towards employing 3D printing [10, 23,24] as a rapid prototyping technique to fabricate micro-scale porous structures of desired complexities, allowing a true engineering of the scaffold [18]. These methods involve the creation of 3D objects using layer by layer deposition approach. Such techniques have successfully been employed in tissue engineering to develop scaffolds based on hard polymeric materials [25,26] and hydrogels [27,28]. The application of scaffolds made from soft polymers or elastomeric materials is desirable when engineering soft tissues [12,29,30]. For the fabrication of elastomeric scaffolds with microfluidic networks, micromoulding and individual layer-by layer assembly techniques have commonly been used [20,31]. However such techniques require the use of complex fabrication technologies and manual assembly for producing large scale structures. Thus the fabrication of 3D elastomeric scaffolds with defined microarchitectural details in cost-effective, scalable manner remains a challenge.

Recently, processes combining 3D printing and moulding have been used for making structured 3D scaffolds. For example, 3D microvascular networks within polymer matrices have been fabricated by 3D printing of sacrificial wax moulds, casting of low viscosity epoxy around the moulds and subsequent removal of the moulds [23,32]. However the use of wax (which has a melting temperature of about 60 °C) limits the materials that can be cast around the mould to form the scaffold since polymers requiring higher temperatures for cross-linking cannot be employed. Furthermore, the complete removal of the sacrificial wax components (which may not be biocompatible) can be challenging, in particular if you have a large 3D structure with complex geometry. Perfusable 3D scaffolds have also been demonstrated in a similar manner by casting extracellular matrix (ECM) containing cells around a 3D printed sacrificial sugar glass lattice and subsequently dissolving the lattice to form vascular networks [24]. However, it is probably difficult to print large 3D structures in the very brittle sugar glass, and the interfilament distance (defined by the printing process) is limited to a minimum of 1 mm. It may therefore not be feasible to use this technique for creating dense vascular channels in large scale structures.

This paper presents a new scalable and general approach for manufacturing structured pores/channels in 3D polymer based scaffolds. The method involves 3D printing (using a commercially available filament based 3D printer) of a sacrificial polyvinyl alcohol (PVA) mould whose geometrical features are designed according to the required vascular channel network. In addition to its biocompatibility, PVA is an ideal material because its water solubility in combination with its high melting temperature (190 °C) makes it robust for subsequent polymer casting and curing steps. A desired polymer is cast around the PVA mould, cross-linked and then the mould is dissolved, leaving behind a structured porous scaffold in the desired polymer material. The fabrication method was here demonstrated for two different polymers, the silicone elastomer polydimethylsiloxane (PDMS), and the synthetic hydrogel poly(2-hydroxyethyl methacrylate) (pHEMA). The scalability of the method was demonstrated by fabricating a 75 cm^3 large PDMS scaffold structure with 16,000 channels. Moreover, it was also shown that the PDMS scaffolds when properly pre-treated could support hepatocyte growth and proliferation for up to 12 days with high viability and proper function.

2. Materials and methods

2.1. Fabrication of structured porous elastomeric scaffolds

The method used to fabricate elastomeric polymer scaffolds with structured channels is schematically presented in Fig. 1. First, a commercial, low-cost 3D filament printer (MakerBot 2X) was used to print

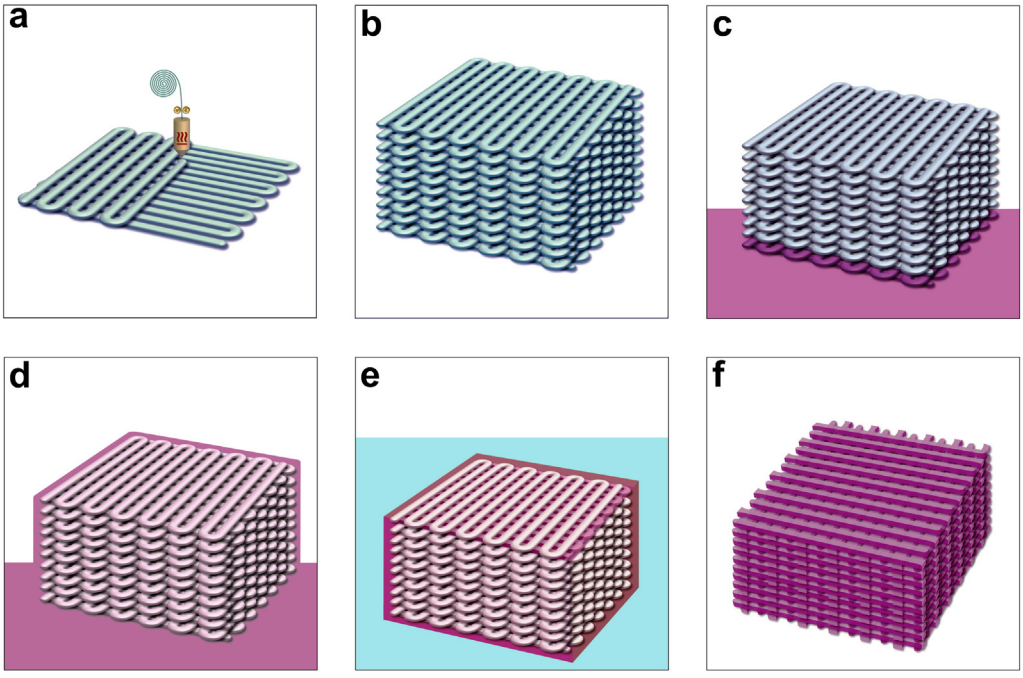

Fig. 1. Schematic illustration of the steps involved in the fabrication of structured porous elastomeric scaffolds. A sacrificial 3D mould was printed in PVA (a, b). The printed PVA mould was transferred into a container containing pre-cured PDMS (c). Vacuum was applied to ensure complete filling of pre-cured PDMS into the pores of the mould (d). Following crosslinking of the PDMS, the sacrificial PVA mould was dissolved in water (e) leaving behind the structured PDMS scaffold (f).

a sacrificial mould. A solid 3D cube of the specified length, width and height was designed using a computer aided design (CAD) software package (SolidWorks 2013). The 3D CAD design was exported as .STL mesh file format for processing using the 3D printer software (Makerware 2.4.1, MakerBot). Commercially available water dissolvable polymer, polyvinyl alcohol (PVA) (MakerBot, USA) filaments were used to print the sacrificial mould. In the printing process a moving nozzle (x- and y-axis control) extrudes a heated polymer filament which then solidifies as it is deposited (Fig. 1(a)). Following deposition of each layer, the mould is lowered (z-axis control) and the extrusion procedure is repeated such that successive layers are built on top of each other to form a 3D object (Fig. 1(b)). The printer settings used for printing PVA moulds are given in Table 1. The extrusion temperature and feed-rates were optimised for printing PVA.

The printing infill density was varied to generate structures with varying porosity. The infill density is the parameter that defines the amount of material filled into the object and subsequently relates to the porosity of the 3D printed structure. The infill density can range from 0% to 100%, where 0% results in a completely hollow object and 100% infill results in a completely solid object. In order to generate structures with different porosities, moulds were printed with infill densities ranging from 20% to 80%. An illustration of the infill patterns and densities that were employed is shown in Supplementary Fig. 1.

The 3D printed microvascular network of the PVA mould was replicated into elastomeric structures of polydimethylsiloxane (PDMS): PDMS pre-polymer solution (Sylgard 184, Dow Corning) was mixed with the curing agent in a 10:1 ratio (as per the manufacturer's guidelines). The mixture was degassed in vacuum and poured into a petri dish containing the printed mould (Fig. 1(c)). PDMS fills the pores of the mould through capillary action and, in addition, vacuum was applied for 2–3 h to ensure complete filling of the micro-channels of the mould with PDMS (Fig. 1(d)). PDMS was cured at a temperature of 60 °C in an oven for 4 h. Once cured, excess PDMS around the mould was removed to expose the PVA layer. This was done to assist the subsequent dissolution of PVA in water: The whole structure was immersed into a water bath (Fig. 1(e)) until the PVA mould was completely dissolved (6 h), and the elastomeric PDMS with microvascular network architecture was obtained (Fig. 1(f)).

Cuboidal PVA moulds of $25 \times 25 \times 10$ mm^3 and $25 \times 25 \times 4$ mm^3 (length × width × height) were printed and used for casting PDMS scaffolds and these scaffolds were used for mechanical testing and cell culturing studies respectively.

2.2. Characterizations of scaffolds

2.2.1. Scanning electron microscopy (SEM) imaging

The structural morphology and microstructure of the printed PVA mould as well as the resulting PDMS porous scaffolds were analysed using scanning electron microscopy (JEOL, Tokyo, Japan). Prior to SEM analysis, moulds and scaffolds were dried in an oven at 50 °C overnight and sputter coated with gold. Samples were then analysed using 12 kV of accelerating voltage. Pore sizes of the moulds and scaffolds were measured from SEM micrographs using ImageJ software. For each sample, ten measurements of pore dimensions were acquired.

For cell-seeded scaffolds, samples were washed with PBS and fixed with 2.5% glutaraldehyde in PBS overnight. Next the samples were dehydrated in a series of ethanol solutions (50%, 70%, 90% and 100%), the samples were further air-dried and then the samples were ready for SEM observation.

Table 1
3D printing parameters used for fabricating sacrificial PVA mould.

3D printing parameters	Settings
Layer height	0.2 mm
Infill pattern	Woodpile or hexagonal
Nozzle temperature	200 °C
Build platform temperature	40 °C
Feed-rate	20 mm/s

2.2.2. Porosity measurement

The porosity of the PDMS scaffold was measured using Eq. (1) as described in the literature [33].

$$\text{Porosity}(\%) = \frac{V - \left(\frac{M}{\rho}\right)}{V} \times 100\% \quad (1)$$

where V is the volume of the scaffold, which is calculated using its outer dimension, M is the mass of the porous PDMS scaffold, and ρ is the density of PDMS (0.965 g/cm^3).

Four scaffolds from each type of scaffold (with dimensions $23 \times 23 \times 6$ mm^3) were dried overnight at 80 °C, and weighed to obtain the mass of the samples. The porosity was then calculated from the weight and the dimensions using Eq. (1).

2.2.3. Mechanical testing

The mechanical properties of dry PDMS scaffolds (with dimensions of $25 \times 25 \times 10$ mm^3) of varying porosity (20–80%) were tested by conducting uniaxial compression tests. A constant compression speed of 0.5 mm/min was applied to each sample using a tensile test machine with a 5 kN load cell (INSTRON Model 4301, Instron Engineering Corporation, Canton, MA, USA). The compressive modulus was estimated from the slope of the stress–strain curve in the elastic region, which was in the range of 12%–20% strain. The stress at 20% strain was obtained. The values reported were an average from four tested samples.

2.2.4. Surface roughness

The surface topography of the PVA mould and PDMS scaffold was visualised using SEM. PDMS scaffold surface roughness was measured using an optical measuring device (Alicona infinite focus). The parameters R_a and R_z were obtained from a standard spectrum of roughness.

2.2.5. Wettability

To assess wettability of the scaffolds, contact angle measurements were carried out on scaffolds before and after treatment with oxygen plasma. The contact angle was measured using the sessile drop method by depositing 3 μl of an ultrapure water drop on the scaffold. Three individual measurements were carried out on three independent scaffolds.

2.2.6. Surface area calculation

To estimate the surface area of the scaffolds, the dimensions of the filaments constituting the mould were acquired from SEM images of the mould. As previously described, the scaffold is formed by printing layers of filaments (with a height of 0.2 mm) organised in the x–y axis. The surface area was calculated from the SEM images of a single layer and then multiplied by the number of layers.

2.3. Culturing cells in scaffolds

2.3.1. Cells

Human hepatoblastoma (HepG2) cells were obtained from the German Collection of Microorganisms and Cell Cultures (DSMZ, Braunschweig, Germany). The cells were maintained in Roswell Park Memorial Institute (RPMI) 1640 growth medium supplemented with 10% foetal bovine serum (FBS, Sigma-Aldrich Chemie GmbH, Switzerland) and 100 μg/ml penicillin and 10 μg/ml streptomycin in a humidified incubator at 37 °C and 5% CO_2. Cells were cultured to confluence in standard polystyrene cell culture flasks, and then released using 0.025% trypsin/EDTA solution. The cell suspension was centrifuged and the cell pellet was washed twice with phosphate buffered saline (PBS) and then re-suspended in fresh growth medium. The cell density was

measured using a haemocytometer and adjusted as required for the seeding on the 3D scaffolds.

2.3.2. Scaffold preparation for cell culture

PDMS scaffolds (fabricated with 80% infill moulds) were frozen in liquid nitrogen and punched into cylindrical scaffolds (having a diameter of 6 mm and height 4 mm) using a tissue puncher (Harris Uni-Core, USA). To render them hydrophilic, the scaffolds were modified with oxygen plasma using a 13.56 MHz RF generator equipped Atto Plasma System (Diener Electronic GmbH, Ebhausen, Germany). Initially the plasma chamber was evacuated to a pressure below 15 Pa, after which oxygen was introduced (pressure stabilization at 30 Pa) and the plasma was ignited (power 50 W) for a duration of 2 min for each side of the scaffold. The treated scaffolds were transferred into an autoclavable glass vial containing sterile water and autoclaved at 120 °C for 20 min for sterilisation. To promote cell attachment to the scaffolds, the scaffolds were coated with 40 μg/ml of Collagen I (Collagen I rat protein, Life Technologies, A1048301) at 4 °C overnight. The scaffolds were washed twice with phosphate buffered saline (PBS) and excess collagen was removed by centrifugation of the samples at 1000 rpm. Finally, the scaffolds were placed in a petri dish containing RPMI medium and incubated inside a humidified incubator at 37 °C and 5% CO_2 for 2 h prior to cell seeding.

2.3.3. Cultivation of HepG2 cells inside the scaffolds

HepG2 cells were cultured in the fabricated scaffolds to evaluate the ability of PDMS 3D constructs to support cell adhesion, proliferation and spreading. For cell seeding a customised cell loading platform was developed as shown schematically in Supplementary Fig. 2. A cell seeding plate with 16 cylindrical holes (having a diameter of 6 mm) and a rectangular support frame was fabricated in 6 mm thick Poly(methyl methacrylate) (PMMA) using a CO_2 laser cutter machine (Epilog Mini 18 Laser, CO 80403, USA). The seeding plate and frame were sterilised by immersion in 0.5 M sodium hydroxide solution for 2 h followed by rinsing in sterile water. The frame and seeding plate were placed inside a sterile petri dish such that the seeding plate was raised and had no direct contact with the petri dish. The collagen coated scaffolds from the incubator were inserted into the holes in the seeding plate. A suspension containing 250,000 cells in 20 μl of media was prepared and loaded into each scaffold. After seeding, the petri plate was incubated at 37 °C for 3 h to allow the cells to attach to the scaffold. Every hour the loading plate was inverted upside down to enable better cell infiltration into the scaffold. Finally the scaffolds were removed from the seeding plate and transferred into a 24 well plate. 1 ml of cell culture medium was added to each well. The medium was refreshed every 2 days and old medium was collected for cellular functionality assays. On days 4, 8 and 12 of the culture period, two scaffolds from each time point were sacrificed and used for live/dead staining.

2.3.4. Biochemical assays

Cell proliferation was estimated using the colorimetric indicator alamarBlue® assay (Life Technologies). The cell-scaffold constructs were transferred into a 24 well plate each containing 1 ml of RPMI and alamarBlue® solution (in a 10:1 ratio) and incubated for 2 h in a humidified incubator at 37 °C. The absorbance of the extracted dye, which is proportional to the number of cells attached to the scaffold, was measured spectrophotometrically using a microplate reader (PerkinElmer, USA) at wavelengths of 570 nm. Three independent scaffolds were measured in triplicates, and the background (i.e., alamarBlue® absorbance measured at day 0) was subtracted.

For the HepG2 functionality test, extracellular concentration of albumin secretion from the HepG2 cells was determined by using an enzyme-linked immunosorbent assay (ELISA) (Bethyl Laboratories, USA) according to the manufacturer's instructions. All samples were measured in triplicates and the standard deviation (SD) of mean was determined from 3 independent scaffolds. The absorbance was measured at 450 nm using a spectrophotometer (PerkinElmer, USA).

2.3.5. Cell imaging

To visualise cell viability in the scaffolds, a live/dead-assay was performed using a live/dead cell imaging kit (Life Technologies LIVE/DEAD® Cell Imaging Kit), which is based on a cell-permeable dye for staining of live cells (excitation/emission 488 nm/515 nm) and a cell-impermeable dye for staining of dead and dying cells (excitation/emission 570 nm/602 nm). Briefly, the cell-laden scaffolds were removed from the culture medium and gently washed with PBS. They were then incubated in the dye solution for 30 min at 37 °C (as per manufacturer's instructions). The scaffolds were imaged using a fluorescence microscope (Zeiss Axio Observer, ZI). 3D reconstructions were compiled from 20 imaged sections (each of 30 μm thickness).

To visualise the cell proliferation and distribution through the cross section of the scaffolds, cell-laden scaffolds were stained with cell-permeable nuclear stain Hoechst 33342 (NucBlue® Live Ready Probes® Reagent, life technologies) for live cell nuclei and ethidium homodimer-1 (life technologies) for dead cell nucleus for 10 min. The scaffolds were then dissected longitudinally using a sterile scalpel and each section was observed under a fluorescence microscope. 3D reconstructions were compiled from 20 imaged sections (each of 30 μm thickness).

An immunofluorescence study was performed to visualise the morphology of cells attached to the scaffold surface: After 12 days of cell growth, the cell-laden scaffolds were immunostained with beta-tubulin as cell cytoskeleton and nucleus. The construct was fixed (4% paraformaldehyde), permeabilized (30 min, 0.1% Triton X-100 in phosphate buffered saline (PBS)), and blocked (30 min, 0.1% Tween 20 and 1% bovine serum albumin in PBS) for unspecific binding of the antibodies. The construct was stained with primary antibody as monoclonal anti-α-tubulin IgG1 (2 h, 1:200, Life Technologies) followed by TO-PRO-3 nuclear stain (1:1000, Life Technologies). The scaffold was then cut through the centre using a sterile scalpel and visualised under a Zeiss ApoTome fluorescence microscope. 3D reconstructions were compiled from 20 imaged sections (each having a thickness of 5 μm).

3. Results

3.1. Scaffold fabrication

Scaffolds were fabricated by casting PDMS around sacrificial moulds printed using two different infill patterns (woodpile and hexagonal) and four different infill densities. Photographs and SEM images of the printed moulds and resulting PDMS scaffolds of the two different infill patterns are shown in Fig. 2. The scaffolds possessed well-defined, porous structures. The square and hexagonal pore structure of both PVA moulds and PDMS scaffolds were observed to be uniform and consistent (Fig. 2(a, b, e, f)). The structural features of the PVA mould are faithfully replicated in the PDMS scaffold (Fig. 2(c, d, g, h)).

The woodpile infill pattern results in structures comprising orthogonal arrays of filaments with the centre-to-centre spacing between adjacent filaments differing based on the chosen infill density (Fig. 3). Infill densities of 20, 40, 60 and 80% produces structures where filaments in a layer had a distances of 1482, 593, 253 and 78 μm respectively. As the infill density increases, the centre-to-centre spacing of the filaments in the PVA mould decreases (Fig. 3a–d). SEM images of the mould showed that the printed PVA filaments have an elliptical cross-section with a width of 400 μm and a height of 200 μm (Supplementary figure). The channels in the resulting PDMS scaffold have an elliptical profile from a cross section view (width 344 μm, height 190 μm) (shown in Supplementary Fig. 5) and a square profile (average side length 344 um) from the top view. The channel dimensions in the PDMS scaffold are slightly smaller than the dimension of the PVA filaments of the mould due to shrinkage of PDMS during the curing process. The channel to channel distance varied from 1.4 mm at 20% infill density down to

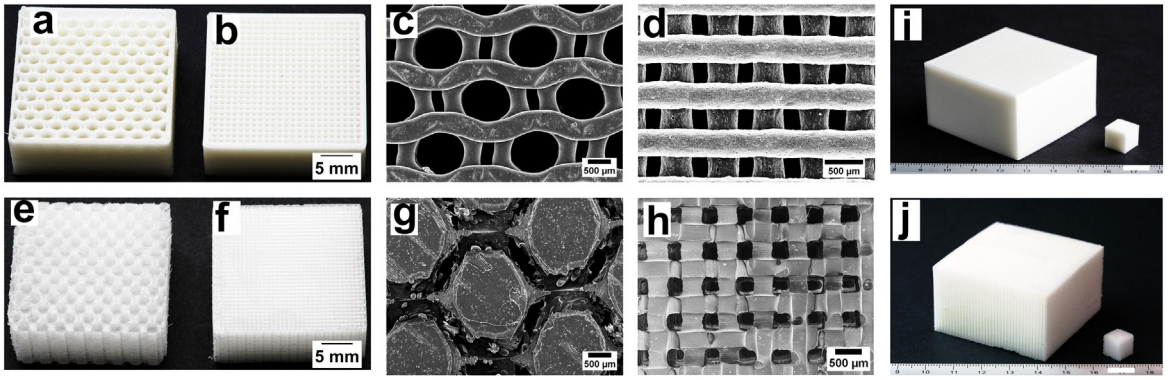

Fig. 2. Photographs of moulds and scaffolds with hexagonal (a, e) and woodpile (b, f) infill patterns. SEM images of moulds and scaffolds with hexagonal (c, g) and woodpile (d, h) infill patterns. (i) Optical image of a 50 layered (1 cm^3 cube) and 150 layered (75 cm^3 cube) 3D printed PVA mould. (j) Optical image of 50 layered (1 cm^3 cube) and 150 layered (75 cm^3 cube) PDMS scaffolds replicated from the mould (i). Scale bar in (i) and (j): 1 cm.

78 μm at 80% infill density of the printed mould. Thus the employed 3D printing technique enables the layer by layer assembly of a different number of PVA filaments forming a porous 3D mould. To demonstrate the scalability of the fabrication process, a larger cubic mould (75 cm^3) was fabricated and employed for generating a replica PDMS scaffold with the same dimensions. Fig. 2(i) shows an image of two cubic moulds of dimensions 1 cm^3 and 75 cm^3 printed using 80% infill settings and Fig. 2(j) shows the resulting PDMS scaffolds. Thus, as demonstrated in Fig. 2, the periodic micro- and macroscale structural patterns of the PVA mould were well replicated in the PDMS scaffolds.

3.2. Scaffold characterisation

3.2.1. Porosity

The experimentally determined porosity of fabricated scaffolds is presented in Fig. 4. The porosity of the scaffolds varied linearly as a function of the infill density of the printed mould from 19.9% porosity at 20% infill up to 81.2% porosity at 80% infill (Fig. 4(a)).

3.2.2. Surface area

The calculated surface areas of a 1 cm^3 fabricated scaffolds of varying porosities are shown in Fig. 4(b). As the infill density of the mould increases from 20% to 80%, there is also a corresponding increase (from 52.5 cm^2/cm^3 to 150.9 cm^2/cm^3, respectively) in the surface area of the channels within the PDMS scaffold volume. As the infill density of the mould increases (Fig. 3(a–d)) the density of channels also increases (Fig. 3(e–h)), which results in a linear increase in the total surface area of the channels (Fig. 4(b)).

3.2.3. Mechanical testing

The assessment of the compressive characteristics of scaffolds is known to play a significant role in many tissue-engineering applications [34]. Compression tests of the scaffolds varying in porosity were performed to assess the stress–strain relationship and evaluate their compressive moduli (Fig. 5). The compressive modulus was determined as the slope of the initial linear portion of the stress vs. strain curve (12–20%). The compressive modulus were determined to be 1.84 ± 0.023, 0.84 ± 0.044, 0.36 ± 0.046 and 0.075 ± 0.047 MPa for the 20, 40, 60, and 80% porosity scaffolds, respectively. Results showed that the energy absorption of the scaffolds is greatly reduced with increasing porosity. There is also a dramatic decrease in the compressive modulus and in the stress at 20% strain with increasing scaffold porosity.

3.2.4. Surface roughness

The roughness of the 3D printed PVA mould and corresponding PDMS scaffold was assessed using SEM. As shown in Fig. 6(a–d), the presence of features such as pillars and grooves visible on the PVA mould are faithfully replicated in the PDMS scaffolds. The roughness of the PDMS scaffold was measured using an optical profilometer. The relative height and surface roughness are shown in the surface profile image (Fig. 6(e)) and the roughness parameters R_a and R_z of the PDMS scaffold surface were measured to be approximately 1.036 μm and 1.32 μm, respectively.

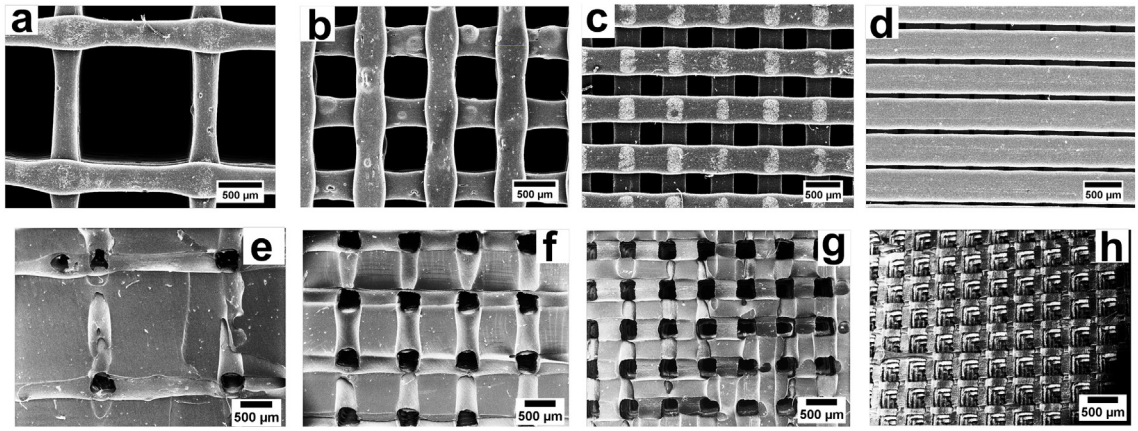

Fig. 3. SEM micrographs of 3D printed PVA moulds of 20, 40, 60 and 80% infill densities (a–d) and corresponding PDMS scaffolds (e–h).

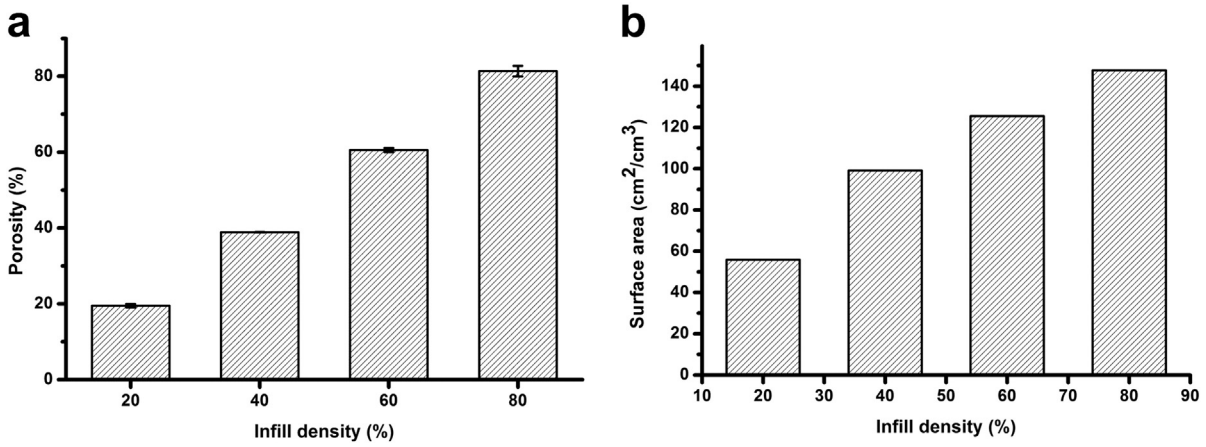

Fig. 4. Measured porosity (error bars = SD, n = 4) (a) and calculated surface to volume ratio (b) of scaffolds fabricated from mould with different infill densities.

3.3. Culturing cells in scaffold

3.3.1. Preparing scaffold for cell culturing (surface treatment)

To enable cell seeding and culturing within a porous scaffolds, it is important to render the scaffold surface hydrophilic [35]. This is required to ensure that the cell suspension and culture media can be absorbed within the scaffold pores. Oxygen plasma treatment was applied to the fabricated scaffolds to achieve this. Using this treatment, the contact angle of the scaffold surface decreased from 122° ± 3.5° to 0° and media was able to infiltrate the pores of the scaffold (Supplementary Fig. 3).

3.3.2. Cell proliferation, viability and function

Following the surface treatment, the scaffolds were prepared for cell culturing, seeded with cells, and incubated as described in Materials and methods. Cell viability and proliferation in the PDMS scaffolds with 80% porosity were investigated over a 12 day culture period using biochemical assays and imaging techniques. Cell proliferation in the scaffold was quantified using the alamarBlue® assay. As shown in Fig. 7(a), the fluorescence intensity increased linearly over the culture period, indicating an increase in the number of cells in the scaffolds with time. The functionality of HepG2 cells cultured on the scaffolds was established by measuring the extracellular albumin production (Fig. 7(b)). There was an increase in albumin production from day 1 to day 12 of the cultures which correlate with the increased cell density in the scaffolds.

Live/dead staining of the cell-scaffold construct was carried out to assess the viability of cells cultured on the scaffolds. Fig. 8 shows the confocal microscopy images of stained HepG2 cells on days 4, 8 and 12 of the culture period. Through the culture period, the density of living cells (stained green) increased. On day 12 of the culture, a confluent layer of live cells was visible on the scaffolds. In all cases, no dead cells were observed, so close to 100% cell viability was maintained throughout the 12 days of culture period.

3.3.3. Cell infiltration and distribution within the scaffolds

At different time points during the culture period, the infiltration and distribution of HepG2 cells within the PDMS scaffolds were investigated. This was done by staining the scaffolds with nuclear stain Hoechst 33342 (NucBlue® Live Ready Probes® Reagent, Life Technologies) for live cell nuclei and ethidium homodimer-1 (life technologies) for dead cell nucleus. To visualise cell distribution through the cross section of the scaffold, it was dissected along its central axis and imaged using fluorescence microscopy. Fig. 9 shows live cell nuclei (stained blue) on the scaffold on days 4, 8 and 12 of the culture. Close to 100% cell viability was observed (no dead cells could be seen) with cells present throughout the cross section of the scaffold by the end of the culture period. Scaffolds acquired from day 4 of the culture showed a higher density of cells closer to the top and bottom face of the scaffold and a sparse density of cells in the central regions of the scaffold. But with longer culture time, cells appeared to proliferate and are seen to be homogenously distributed throughout the channels of the scaffolds at days 8 and 12.

Immunostaining of the scaffold was carried out to visualise the morphology of cells cultured on the scaffolds. Fig. 10 shows a homogeneous and confluent distribution of cells in the central region of the scaffold,

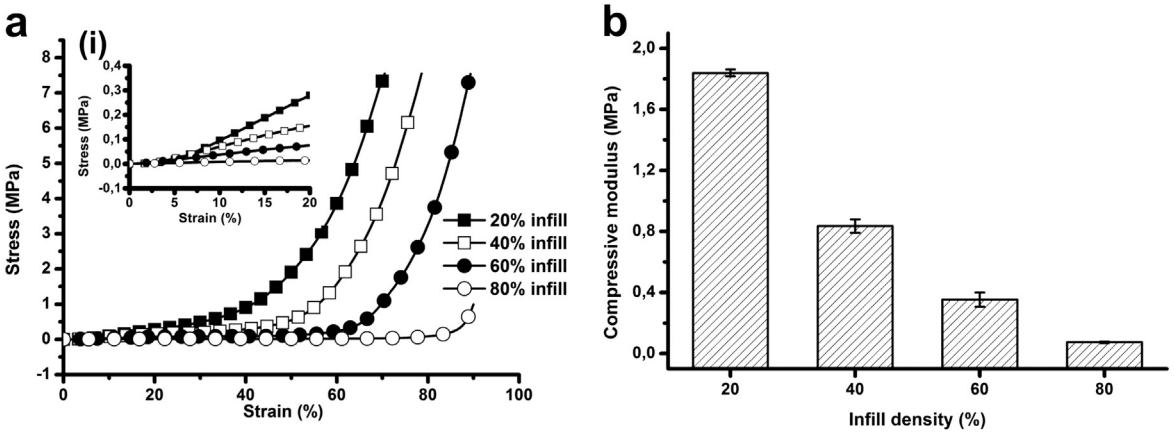

Fig. 5. (a) Stress–strain curves at 4 N load for different scaffolds, (b) compressive moduli of different PDMS scaffolds (error bars = standard deviation of 4 samples (n = 4)).

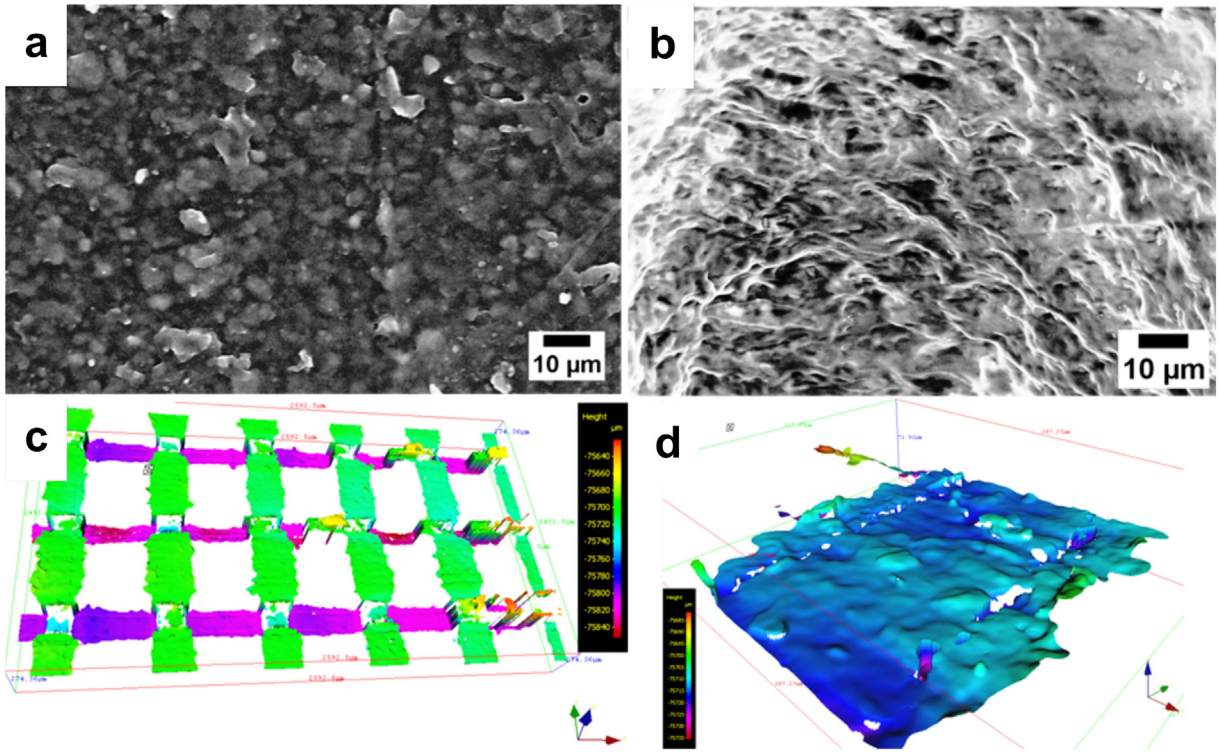

Fig. 6. Surface roughness analysis: SEM images showing microfeatures in the PVA mould surface (a) and PDMS scaffold (b, c & d). Surface profile image of PDMS scaffold surface generated from optical profilometer (c) and zoom in of image c (d).

highlighting the cytoskeleton beta-tubulin (green) and cell nucleus (red). After 12 days of cell culture the cells were uniformly distributed with high density of live cell in the centre of the scaffold. Immunofluorescence staining of the beta-tubulin demonstrated that the cells were well attached to the surface with a spread-out cell morphology.

HepG2 cell adhesion on scaffold was also investigated through SEM as shown in the Supplementary Fig. 5(a, b & c). After 4 days of culture, the interaction between cells and the scaffold surface was examined. Cells cultured on PDMS scaffold formed a well spread morphology and exhibited excellent cell adhesion.

4. Discussion

In this paper, a new scalable and reproducible technique for fabricating 3D polymer scaffolds with defined micro-architectures has been presented. The technique is simple and involves casting of a desired polymer material within a 3D printed water-soluble PVA mould, which defines the microarchitecture/geometry of pores or channels within the scaffold (Figs. 1–3). 3D printing parameters were optimised to enable the production of reproducible moulds with high yield. The technique was applied to fabricate 'woodpile' like scaffolds with regularly spaced aligned polymer filaments in the x and y directions. Scaffolds of porosities ranging from 20 to 80% and channel to channel distances ranging from 78 μm to 1482 μm were fabricated by specifying the infill density of the moulds. Scaffolds with hexagonal micro-features were also obtained by using moulds with hexagonal infill patterns. The dimensions of the channels formed in the PDMS replica scaffolds were ellipsoidal shaped with dimensions (344 μm × 190 μm) that were slightly smaller than that of the filaments in the printed mould (400 μm × 200 μm), due to shrinkage during elastomer curing.

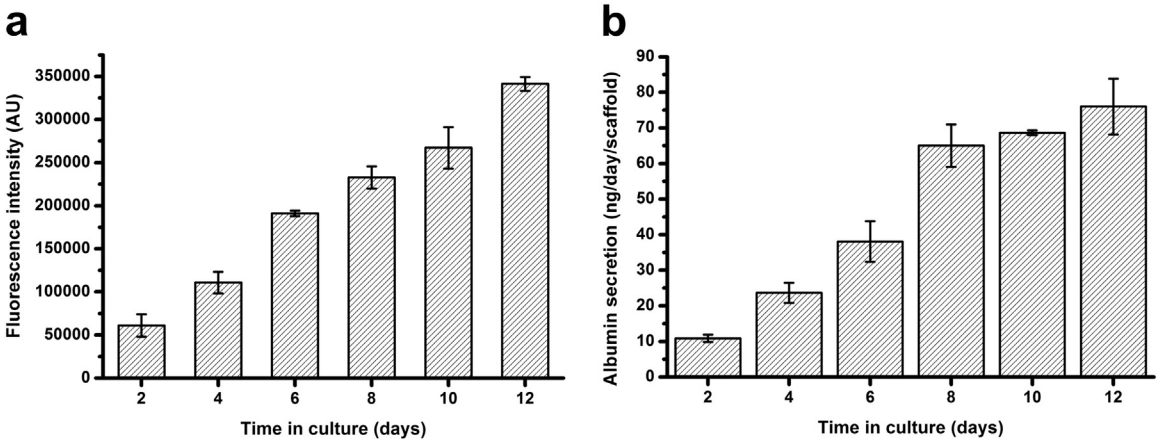

Fig. 7. (a) Change in alamarBlue® florescence intensity of scaffolds over culture time. The fluorescence intensity is proportional to the amount of cells. (b) Albumin production of HepG2 cells grown in PDMS scaffolds over 12 days of culture. Error bars indicate standard deviation of 3, independent scaffolds.

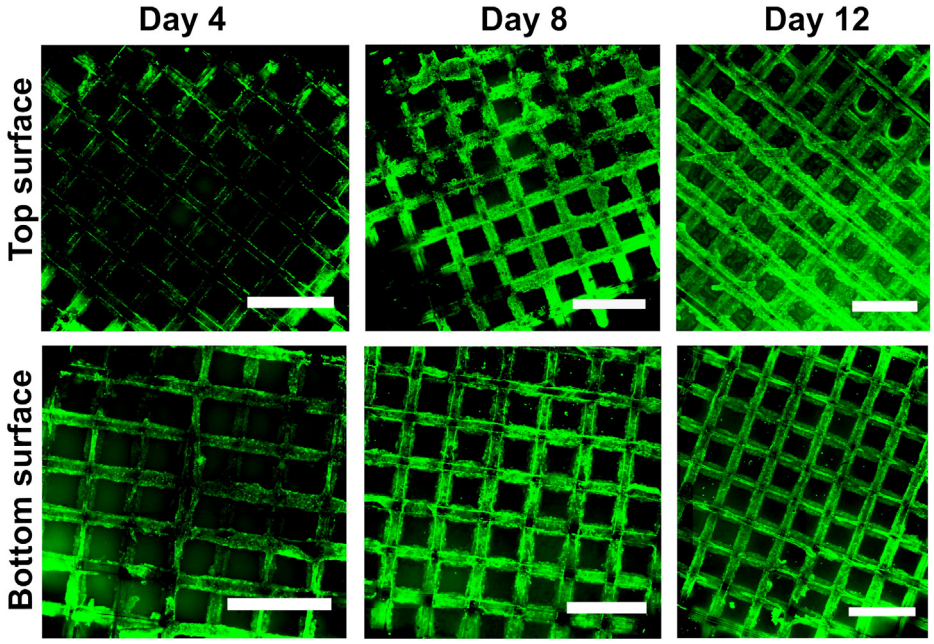

Fig. 8. Live/dead staining of HepG2 cells grown on the top and bottom parts of the PDMS scaffold for 4, 8 and 12 days. Scale bars represent 1 mm. (For interpretation of the references to colour in this figure, the reader is referred to the web version of this article.)

We used the biocompatible elastomeric polymer PDMS to demonstrate the ease of fabrication and scaling of scaffold structure, and furthermore showed that it has potential as a scaffold for growth of liver cells. However, the method has general applicability, meaning that other mouldable materials can be structured in a similar manner. To prove this point, poly-2-hydroxyethyl methacrylate (pHEMA) hydrogel scaffolds were produced by monomer/crosslinker casting around PVA mould, photocrosslinking (Supplementary Fig. 4, and Material and method in the Supplementary section) and subsequent dissolution of the PVA mould.

The silicone elastomer PDMS is optically clear, and, in general, inert, non-toxic, and non-flammable. Its applications range from contact lenses and medical devices to additives in cosmetics and food products. PDMS is also widely used as a material for microfluidic cell culturing and the high number of publications using it indicates that it is a biocompatible material [36]. In general the effects of PDMS or silicones on cells need to be evaluated on a case by case situation, as PDMS in some situations has subtle effect on gene expression [37], but we clearly show here that the fabricated PDMS elastomer scaffold supports HepG2 growth and function (Figs. 7–10). This type of elastomer scaffold could be used as a part of a life support system (LSS), e.g., an extracorporeal liver [38] to temporarily relieve liver disease patients. In such application PDMS offers several advantages: 1) It is easy to fabricate PDMS scaffold structures using the PVA sacrificial moulding method presented here. 2) PDMS is a structurally strong material for building large meshes (Fig. 2j). 3) PDMS is easy to sterilise by autoclavation (in contrast to some hydrogels). 4) In contrast to hydrogels and many biodegradable materials PDMS does not shrink, swell or warp significantly with time meaning that rational fluidics optimisation can be done as well as robust fluidic connections for perfusions. 5) There are FDA approved medical grade silicone elastomers which should be compatible with the here described fabrication method.

It is well recognised that in order to be of clinical relevance, tissue constructs must be scaled up to the macroscale, not only in length and width, but also in thickness [20]. The presented fabrication method overcomes existing challenges in creating thicker constructs in a simple and reproducible manner by using precision assembly technology to control the micro-architectural details. The scalability of the process was demonstrated by producing a 75 cm^3 large scaffold structure with 16,000 channels with a channel to channel distance of only 78 μm (Fig. 2(j)). To our knowledge this is the largest scaffold ever to be produced with such small features sizes and with so many structured channels. Thus the process enables a more efficient scale up of scaffolds both in size and in throughput, while also allowing versatility in the implementation of 3D microarchitectural designs.

It is well established that the micro-roughness of a scaffold surface plays an important role in cell attachment and proliferation [39–42]. For this reason, the topological features of the scaffold were analysed using SEM to measure the surface roughness. Geometrical and topological features of the 3D printed PVA mould (Fig. 6a and b) were well

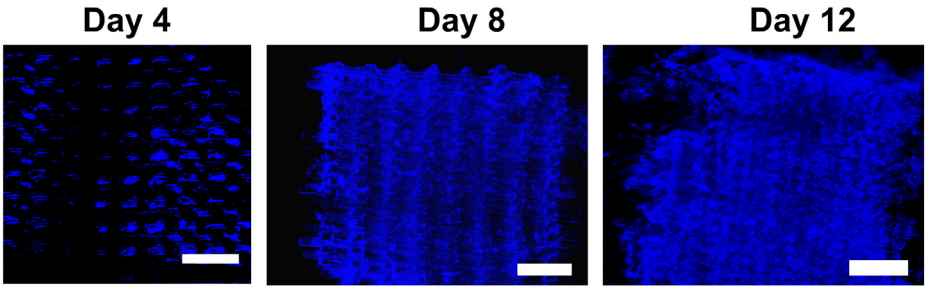

Fig. 9. Visualisation of cell distribution through the central section of the scaffold stained with NucBlue® (live cells: blue) and ethidium Homodimer-1 (EthD-1) (dead stain: red) on days 4, 8, and 12 of HepG2 cell culturing. Scale bars: 1 mm. (For interpretation of the references to colour in this figure legend, the reader is referred to the web version of this article.)

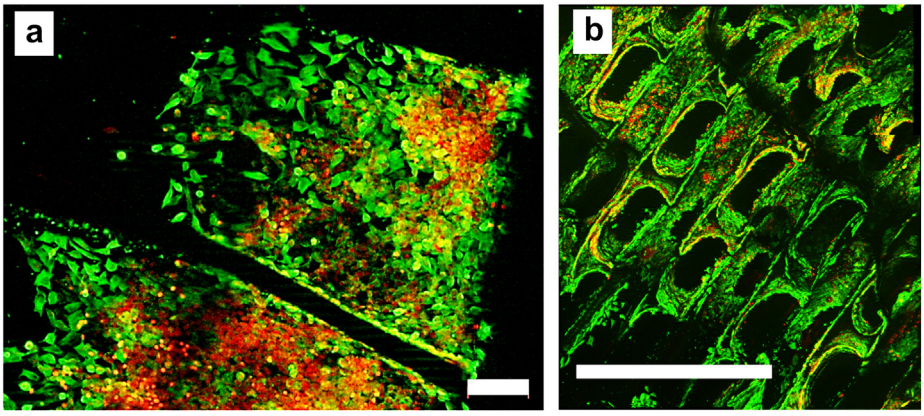

Fig. 10. HepG2 cell morphology and attachment to PDMS scaffold using immunostaining (a & b). Cell cytoskeleton beta tubulin (green) and nucleus (red). (a) Top surface of the scaffold. (b) Longitudinal cross section of the scaffold. Scale bar of image: a) with 100 μm and b) with 1 mm. (For interpretation of the references to colour in this figure legend, the reader is referred to the web version of this article.)

replicated in the PDMS scaffold (Fig. 6c and d), giving the scaffold micro- and nano-scale roughness. Such micro- and nano-scale roughness can be an advantage for cell attachment and proliferation [43]. Our results are in agreement with this: We observed confluent layer of well-attached cells with spread-out cell morphology (Fig. 10).

It is well known that cells respond to the material on which they grow, both in terms of cytoskeleton, cell morphology, cell differentiation and function [45,46]. The mechanical properties of the fabricated scaffolds of varying porosities were therefore characterised. The compressive modulus of the scaffolds were estimated to be 1.84, 0.84, 0.34, 0.075 MPa for 20, 40, 60 and 80% porous scaffolds, respectively. The inverse relationship between scaffold porosity and compressive modulus is expected because scaffold with a higher porosity has less material/mass to resist applied load and therefore has a lower compressive modulus. If the stiffness of the PDMS scaffold should be a problem it can be adjusted by changing the ratio of pre-polymer to curing agent [46] or by selecting hydrogel materials such as pHEMA (Supplementary Fig. 4) could be used for casting the scaffold.

A highly available surface area in a scaffold can provide high ligand density for initial cell attachment and proliferation [47]. We chose to use the scaffold with the highest porosity (80%) for culturing cells since it has the lowest compressive modulus, enables better mass transport, and has the highest specific surface area (Fig. 4b) for cell attachment.

Until now it has been a challenge to maintain viable cells within the inner cores of thick engineered tissue constructs due to insufficient oxygen and nutrient levels [33]. To regenerate artificial tissues a homogeneous cell distribution should be maintained inside the porous scaffold structure [48,49]. The scaffolds presented in this work were able to sustain cells with 100% viability throughout the 12 day culture period. Metabolic assays and total cell DNA quantification assays do not give information on cell infiltration and distribution inside the scaffold. In order to visualise this aspect, the cell nucleus stained scaffolds were imaged at the top, bottom and cross sectional surfaces (Fig. 9). Cells were seen to be uniformly distributed throughout the channels of the scaffolds and along the cross sectional length of the scaffold. The achieved homogeneity can be attributed to the following: Firstly, the cell loading procedure employed ensures an even distribution of cells throughout the scaffolds. Secondly, the parallel and perpendicular structured channels in the scaffold allow sufficient oxygen and nutrient mass transport into the scaffold which promotes cell survival and proliferation. Thus at the end of the culture period, cells were seen to be uniformly distributed throughout the scaffolds and along the cross sectional length of the scaffold. Results from immunostaining clearly showed good HepG2 cell morphology and attachment to the scaffold surface (Fig. 10). Cell functionality was assessed by measuring albumin secretion of cells in scaffolds over time (Fig. 7b). The increase in albumin secretion through the culture period indicates that the cells were able to maintain their functionally while cultured in the presented 3D scaffold.

5. Conclusions

In this study, we have demonstrated a new technique for fabricating scaffolds by 3D printing a sacrificial water dissolvable PVA mould, casting polymer around it and subsequently dissolving the sacrificial mould, leading to structured scaffolds. Different designs of PDMS scaffolds were successfully prepared, and the fabrication technique allowed the tuning of physical and mechanical properties by controlling the 3D printing parameter. By observing the biological activity of the hepatocytes in the scaffold we conforms that along with maintaining very high cellular viability the scaffold could also support high level of cellular albumin secretion throughout the cultivation period. After 12 days of cell culturing we observed a very high density of cells, homogeneously distribution across the scaffold due to good mass and oxygen transport into the scaffold. The fabrication method can also be applied to other synthetic or natural polymers as demonstrated by fabricating scaffolds in the hydrogel pHEMA. Furthermore, as we have demonstrated, the fabricated scaffold can be scaled up to sizes relevant for bioartificial organs. In conclusion, the described process is scalable, compatible with cell culture, rapid, and inexpensive.

Supplementary data to this article can be found online at http://dx.doi.org/10.1016/j.msec.2015.06.002.

Acknowledgments

This work has been financially supported by EU project NanoBio4Trans ("A new nanotechnology-based paradigm for engineering vascularised liver tissue for transplantation", grant no: 304842). We thank K. Kuldeep and Aradhya Mallikarjunaiah Chetan for their great support in carrying out with the fabrication of 3D scaffolds and Jesper Scheel for taking photographs of the large scaffold.

References

[1] L.G. Griffith, M.A. Swartz, Capturing complex 3D tissue physiology in vitro, Nat. Rev. Mol. Cell Biol. 7 (3) (Mar 2006) 211–224.
[2] K.C. Rustad, M. Sorkin, B. Levi, M.T. Longaker, G.C. Gurtner, Strategies for organ level tissue engineering, Organogenesis 6 (3) (2010) 151–157.
[3] A. Khademhosseini, R. Langer, J. Borenstein, J.P. Vacanti, Microscale technologies for tissue engineering and biology, Proc. Natl. Acad. Sci. U. S. A. 103 (8) (Feb 2006) 2480–2487.
[4] A. Khademhosseini, J.P. Vacanti, R. Langer, Progress in tissue engineering, Sci. Am. 300 (2009) 64–71.
[5] D.M. Hoganson, H.I. Pryor, J.P. Vacanti, Tissue engineering and organ structure: a vascularized approach to liver and lung, Pediatr. Res. 63 (5) (May 2008) 520–526.

[6] T. Lu, Y. Li, T. Chen, Techniques for fabrication and construction of three-dimensional scaffolds for tissue engineering, Int. J. Nanomedicine 8 (Jan 2013) 337–350.
[7] H.A. Almeida, P.J. Bártolo, Design of tissue engineering scaffolds based on hyperbolic surfaces: structural numerical evaluation, Med. Eng. Phys. 36 (8) (Aug 2014) 1033–1040.
[8] R. Langer, Perspectives and challenges in tissue engineering and regenerative medicine, Adv. Mater. 21 (32–33) (Sep 2009) 3235–3236.
[9] M.D. Guillemette, H. Park, J.C. Hsiao, S.R. Jain, B.L. Larson, R. Langer, L.E. Freed, Combined technologies for microfabricating elastomeric cardiac tissue engineering scaffolds, Macromol. Biosci. 10 (11) (Nov 2010) 1330–1337.
[10] C.G. Jeong, S.J. Hollister, Mechanical and biochemical assessments of three-dimensional poly(1,8-octanediol-co-citrate) scaffold pore shape and permeability effects on in vitro chondrogenesis using primary chondrocytes, Tissue Eng. A 16 (12) (2010) 3759–3768.
[11] M.E. Kolewe, H. Park, C. Gray, X. Ye, R. Langer, L.E. Freed, 3D structural patterns in scalable, elastomeric scaffolds guide engineered tissue architecture, Adv. Mater. 25 (32) (Aug 2013) 4459–4465.
[12] S.J. Hollister, Scaffold design and manufacturing: from concept to clinic, Adv. Mater. 21 (32–33) (Sep 2009) 3330–3342.
[13] A. G. Mikos, G. Sarakinos, J. P. Vacanti, R. S. Langer, and L. G. Cima, "Biocompatible polymer membranes and methods of preparation of three dimensional membrane structures." Google Patents, 1996.
[14] H. Lo, M.S. Ponticiello, K.W. Leong, Fabrication of controlled release biodegradable foams by phase separation, Tissue Eng. 1 (1) (Jan 1995) 15–28.
[15] D.J. Mooney, D.F. Baldwin, N.P. Suh, J.P. Vacanti, R. Langer, Novel approach to fabricate porous sponges of poly(D,L-lactic-co-glycolic acid) without the use of organic solvents, Biomaterials 17 (14) (Jul 1996) 1417–1422.
[16] K. Whang, K.E. Healy, A novel method scaffolds to fabricate bioabsorbable, 36 (4) (1995) 837–842.
[17] A. Saraf, G. Lozier, A. Haesslein, F.K. Kasper, R.M. Raphael, L.S. Baggett, A.G. Mikos, Fabrication of nonwoven coaxial fiber meshes by electrospinning, Tissue Eng. C Methods 15 (3) (Sep 2009) 333–344.
[18] B. Derby, Printing and prototyping of tissues and scaffolds, Science 338 (6109) (Nov 2012) 921–926.
[19] W.-Y. Yeong, C.-K. Chua, K.-F. Leong, M. Chandrasekaran, Rapid prototyping in tissue engineering: challenges and potential, Trends Biotechnol. 22 (12) (Dec 2004) 643–652.
[20] X. Ye, L. Lu, M.E. Kolewe, K. Hearon, K.M. Fishcher, J. Coppeta, L.E. Freed, Scalable Units for Building Cardiac Tissue, Advanced Materials (Deerfield Beach, Fla.) 26 (42) (2014) 7202–7208.
[21] A.P. Golden, J. Tien, Fabrication of microfluidic hydrogels using molded gelatin as a sacrificial element, Lab Chip 7 (6) (Jun 2007) 720–725.
[22] J. He, Y. Wang, Y. Liu, D. Li, Z. Jin, Layer-by-layer micromolding of natural biopolymer scaffolds with intrinsic microfluidic networks, Biofabrication 5 (2) (Jun 2013) 025002.
[23] D. Therriault, S.R. White, J.A. Lewis, Chaotic mixing in three-dimensional microvascular networks fabricated by direct-write assembly, Nat. Mater. 2 (4) (Apr 2003) 265–271.
[24] J.S. Miller, K.R. Stevens, M.T. Yang, B.M. Baker, D.T. Nguyen, D.M. Cohen, E. Toro, A.A. Chen, P.A. Galie, X. Yu, R. Chaturvedi, S.N. Bhatia, C.S. Chen, Rapid casting of patterned vascular networks for perfusable engineered three-dimensional tissues, Nat. Mater. 11 (9) (Sep 2012) 768–774.
[25] J.M. Sobral, S.G. Caridade, R.A. Sousa, J.F. Mano, R.L. Reis, Three-dimensional plotted scaffolds with controlled pore size gradients: effect of scaffold geometry on mechanical performance and cell seeding efficiency, Acta Biomater. 7 (3) (Mar 2011) 1009–1018.
[26] H.A. Declercq, T. Desmet, P. Dubruel, M.J. Cornelissen, The Role of Scaffold Architecture and Composition on the Bone Formation by Adipose-derived Stem Cells, vol. 202014. 434–445.
[27] L.E. Bertassoni, J.C. Cardoso, V. Manoharan, A.L. Cristino, N.S. Bhise, W.A. Araujo, P. Zorlutuna, N.E. Vrana, A.M. Ghaemmaghami, M.R. Dokmeci, A. Khademhosseini, Direct-write bioprinting of cell-laden methacrylated gelatin hydrogels, Biofabrication 6 (2) (Apr 2014) 024105.
[28] R. Gauvin, Y.-C. Chen, J.W. Lee, P. Soman, P. Zorlutuna, J.W. Nichol, H. Bae, S. Chen, A. Khademhosseini, Microfabrication of complex porous tissue engineering scaffolds using 3D projection stereolithography, Biomaterials 33 (15) (May 2012) 3824–3834.
[29] L.E. Freed, G.C. Engelmayr, J.T. Borenstein, F.T. Moutos, F. Guilak, Advanced material strategies for tissue engineering scaffolds, Adv. Mater. 21 (32–33) (Sep 2009) 3410–3418.
[30] J. Gao, P.M. Crapo, Y. Wang, Macroporous elastomeric scaffolds with extensive micropores for soft tissue engineering, Tissue Eng. 12 (4) (Apr 2006) 917–925.
[31] H. Park, B.L. Larson, M.D. Guillemette, S.R. Jain, C. Hua, G.C. Engelmayr, L.E. Freed, The significance of pore microarchitecture in a multi-layered elastomeric scaffold for contractile cardiac muscle constructs, Biomaterials 32 (7) (Mar 2011) 1856–1864.
[32] D. Therriault, R.F. Shepherd, S.R. White, J.A. Lewis, Fugitive inks for direct-write assembly of three-dimensional microvascular networks, Adv. Mater. 17 (4) (Feb 2005) 395–399.
[33] Q. Zhang, H. Luo, Y. Zhang, Y. Zhou, Z. Ye, W. Tan, M. Lang, Fabrication of three-dimensional poly(ε-caprolactone) scaffolds with hierarchical pore structures for tissue engineering, Mater. Sci. Eng. C 33 (4) (May 2013) 2094–2103.
[34] S.J. Hollister, Porous scaffold design for tissue engineering, Nat. Mater. 4 (July 2005) 518–524.
[35] S. Oh, Fabrication and characterization of hydrophilic poly(lactic-co-glycolic acid)/poly(vinyl alcohol) blend cell scaffolds by melt-molding particulate-leaching method, Biomaterials 24 (22) (Oct 2003) 4011–4021.
[36] E. Berthier, E.W.K. Young, D. Beebe, Engineers are from PDMS-land, biologists are from Polystyrenia, Lab Chip 12 (7) (Apr 2012) 1224–1237.
[37] J.M. Łopacińska, J. Emnéus, M. Dufva, Poly(dimethylsiloxane) (PDMS) affects gene expression in PC12 cells differentiating into neuronal-like cells, PLoS One 8 (1) (Jan 2013) e53107.
[38] A.J. Strain, J.M. Neuberger, A bioartificial liver—state of the art, Science 295 (5557) (Feb 2002) 1005–1009.
[39] R.G. Flemming, C.J. Murphy, G.A. Abrams, S.L. Goodman, P.F. Nealey, Effects of synthetic micro- and nano-structured surfaces on cell behavior, Biomaterials 20 (6) (Mar 1999) 573–588.
[40] L. Marcotte, M. Tabrizian, Sensing surfaces: challenges in studying the cell adhesion process and the cell adhesion forces on biomaterials, IRBM 29 (2–3) (Apr 2008) 77–88.
[41] X. Liu, J.Y. Lim, H.J. Donahue, R. Dhurjati, A.M. Mastro, E.A. Vogler, Influence of substratum surface chemistry/energy and topography on the human fetal osteoblastic cell line hFOB 1.19: Phenotypic and genotypic responses observed in vitro, Biomaterials 28 (31) (Nov 2007) 4535–4550.
[42] S. Sant, A. Khademhosseini, Fabrication and characterization of tough elastomeric fibrous scaffolds for tissue engineering applications, Conf. Proc. IEEE Eng. Med. Biol. Soc. 2010 (Jan 2010) 3546–3548.
[43] A. Dolatshahi-Pirouz, M. Nikkhah, K. Kolind, M.R. Dokmeci, A. Khademhosseini, Micro- and nanoengineering approaches to control stem cell-biomaterial interactions, J. Funct. Biomater. 2 (4) (Jun 2011) 88–106.
[45] T. Yeung, P.C. Georges, L.A. Flanagan, B. Marg, M. Ortiz, M. Funaki, N. Zahir, W. Ming, V. Weaver, P.A. Janmey, Effects of substrate stiffness on cell morphology, cytoskeletal structure, and adhesion, Cell Motil. Cytoskeleton 60 (1) (Jan 2005) 24–34.
[46] B. Trappmann, J.E. Gautrot, J.T. Connelly, D.G.T. Strange, Y. Li, M.L. Oyen, M.A. Cohen Stuart, H. Boehm, B. Li, V. Vogel, J.P. Spatz, F.M. Watt, W.T.S. Huck, Extracellular-matrix tethering regulates stem-cell fate, Nat. Mater. 11 (7) (Jul 2012) 642–649.
[47] F.J. O'Brien, B.A. Harley, I.V. Yannas, L.J. Gibson, The effect of pore size on cell adhesion in collagen-GAG scaffolds, Biomaterials 26 (4) (Feb 2005) 433–441.
[48] P. Thevenot, A. Nair, J. Dey, J. Yang, L. Tang, Method to analyze three-dimensional cell distribution and infiltration in degradable scaffolds, Tissue Eng. C Methods 14 (4) (Dec 2008) 319–331.
[49] H. Lee, S. Ahn, L.J. Bonassar, W. Chun, G. Kim, Cell-laden poly(ε-caprolactone)/alginate hybrid scaffolds fabricated by an aerosol cross-linking process for obtaining homogeneous cell distribution: fabrication, seeding efficiency, and cell proliferation and distribution, Tissue Eng. C Methods 19 (10) (Oct. 2013) 784–793.